Mechanism of 30S subunit recognition and modification by the conserved bacterial ribosomal RNA methyltransferase RsmI

Mohamed I. Barmada[1,2], Erin N. McGinity[1], Suparno Nandi[1], Debayan Dey[1], Natalia Zelinskaya[1], George M. Harris[3], Lindsay R. Comstock[3], Christine M. Dunham[4] and Graeme L. Conn[1]*

[1]Department of Biochemistry, Emory University School of Medicine, Atlanta, Georgia, 30322, USA
[2]Graduate Program in Biochemistry, Cell and Developmental Biology, Emory University, Atlanta, Georgia, 30322, USA
[3]Department of Chemistry, Wake Forest University, Winston-Salem, North Carolina, 27106, USA
[4]Department of Chemistry, Emory University, Atlanta, Georgia, 30322, USA

*To whom correspondence should be addressed. Email: gconn@emory.edu

Competing Interest Statement: The authors declare no competing interests.

Keywords: Ribosome, methylation, 30S subunit, helix 44, methyltransferase, substrate recognition

Abstract

Ribosomal RNA (rRNA) modifications are important for ribosome function and can influence bacterial susceptibility to ribosome-targeting antibiotics. The universally conserved 16S rRNA nucleotide C1402, for example, is the only 2'-*O*-methylated nucleotide in the bacterial small (30S) ribosomal subunit and this modification fine tunes the shape and structure of the peptidyl tRNA binding site. The Cm1402 modification is incorporated by the conserved bacterial 16S rRNA methyltransferase RsmI, but it is unclear how RsmI is able to recognize its 30S substrate and specifically modify its buried target nucleotide. We determined a 2.42 Å resolution cryo-EM structure of the RsmI-30S complex and, with accompanying functional analyses, show that RsmI anchors itself to the 30S subunit through multiple contacts with a conserved 16S rRNA tertiary surface present only in the assembled subunit. This positions RsmI to induce an extensive h44 distortion to access C1402 that is unprecedented among 16S rRNA methyltransferases characterized to date. These analyses also reveal an essential contribution to 30S subunit interaction made by the previously structurally uncharacterized RsmI C-terminal domain, RsmI-induced RNA-RNA interactions with C1402, and an unappreciated dependence on a divalent metal ion for catalysis, marking RsmI as the first of a distinct class of metal- and SAM-dependent RNA *O*-methyltransferases. This study significantly expands our mechanistic understanding of how intrinsic bacterial methyltransferases like RsmI modify their rRNA targets. Further, recognition of distant ribosome features and extensive unfolding of a critical rRNA functional center point to a potential role in accurate 30S subunit biogenesis.

Introduction

One hallmark of accurate bacterial ribosome biogenesis is methylation of select nucleotides at the functional centers of both ribosomal subunits (1). These modified nucleotides play important roles in the process of individual subunit assembly (2), translational fidelity (3, 4), ribosome-ligand interactions (5), and antibiotic susceptibility (6). Among the conserved methylated nucleotides in the small (30S) ribosomal subunit, C1402 is the only 16S rRNA nucleotide to be methylated at both its nitrogenous base (on the N4 atom to form m^4C1402) and its ribose 2'-OH (to form Cm1402). The conserved S-adenosyl-L-methionine (SAM)-dependent methyltransferase RsmI is responsible for incorporating the latter modification (7), which is the only conserved ribose 2'-O-methyl modification in the bacterial 30S subunit.

The dual methylated C1402 (m^4Cm1402) is located within helix 44 (h44), forming a non-canonical base pair with A1500 (8). m^4Cm1402 plays important roles in fine tuning the shape and structure of the 30S subunit peptidyl tRNA binding site (P site) and makes a direct contact with the mRNA codon (4, 9). Loss of RsmI, and thus the Cm1402 modification, results in defects in translational fidelity, including an increase in stop codon readthrough, a decrease in mRNA reading frame

maintenance (7), and increased sensitivity to certain antibiotics (6). The level of C1402 2'-O-methylation appears dynamically regulated in response to antibiotic stress (10) and also contributes to sensitivity to other stresses such as oxidative stress (11). While much is known about the functional impacts of the Cm1402 modification, how the ribose methylation is incorporated by RsmI is currently less well understood.

RsmI functions as a dimer to incorporate the Cm1402 modification within the assembled 30S subunit but is unable to modify naked 16S rRNA or 70S ribosomes *in vitro* (7, 12). These observations imply that RsmI likely acts on the 30S subunit late in biogenesis but before 70S ribosome assembly, where h44 becomes further occluded by the 50S subunit. While RsmI therefore presumably relies on conserved features of the assembled 30S subunit or late assembly intermediate for substrate recognition, the enzyme must also be able to manipulate the folded architecture of the 16S rRNA h44 to access the relatively deeply buried C1402 residue. However, why RsmI acts as a dimer and requires the mature or near mature 30S subunit as its substrate, and how RsmI distorts the h44 structure to access C1402 for modification are currently unknown.

To uncover the molecular basis behind C1402 recognition and modification by RsmI, we determined the structure of the *Escherichia coli* RsmI-30S subunit complex to a global resolution of 2.42Å using cryogenic electron microscopy (cryo-EM) complemented by functional studies of key RsmI residues. These studies reveal that RsmI anchors itself to the 30S subunit by binding to a highly conserved tertiary surface of 16S rRNA helices present in the assembled 30S subunit, relying on both protomers of its dimeric structure for distinct but equally essential roles in substrate recognition. One RsmI protomer extensively distorts h44 to access C1402, while the other recognizes a distant structural feature of the 30S subunit via a functionally critical but previously structurally undefined C-terminal domain (CTD). These studies additionally reveal catalysis of C1402 methylation by RsmI to be a divalent metal ion-dependent process, a unique feature among 16S rRNA methyltransferases characterized to date. Overall, this work reveals an extraordinarily high degree of rRNA manipulation by an rRNA methyltransferase and provides key insights into both the mechanism of action of intrinsic ribosomal 16S rRNA methyltransferases as well as pointing to their potential contributions to 30S subunit biogenesis.

Results

Structure of the RsmI-30S subunit complex.

The 30S subunit lacking the Cm1402 modification ("30S-Δ*rsmI*") was isolated from an *E. coli* Δ*rsmI* strain and confirmed as a suitable substrate for RsmI using an *in vitro* methyltransferase assay (**Supplementary Fig. S1**). The RsmI-30S complex was prepared by mixing 30S-Δ*rsmI*, purified recombinant RsmI and the SAM analog 5'-(diaminobutyric acid)-N-iodoethyl-5'-deoxyadenosine

ammonium hydrochloride ("NM6") in a 1:3:30 ratio. Through the action of RsmI, NM6 becomes covalently attached to the substrate in an alkylation reaction (13, 14), trapping the enzyme-30S substrate complex in an immediately post-catalytic state by virtue of the enzyme's affinity for both substrate and co-substrate analog.

With this complex, we used single-particle cryo-EM to generate a map of the entire RsmI-30S subunit complex as well as a focused map of RsmI and its adjacent 16S rRNA binding interface on the 30S subunit to global resolutions of 2.42 Å and 2.55 Å, respectively (**Fig. 1A**,**B**; **Supplementary Figs. S2**, **S3**, and **Table S1**). Together, these maps enabled the full modelling of the structure of the RsmI-

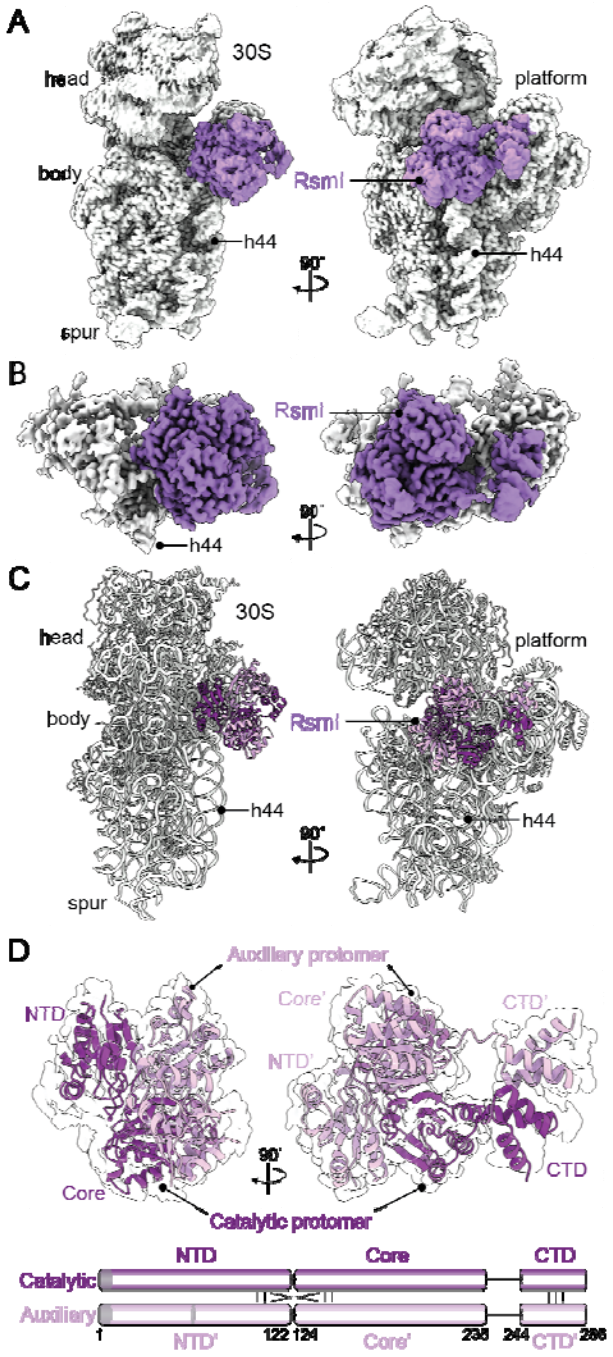

Figure 1. **Structure of the RsmI-30S subunit complex**. **A**. Sharpened cryo-EM map of the RsmI-30S complex. **B**. Sharpened cryo-EM map of RsmI and its 16S rRNA binding surface on the 30S subunit. **C**. Model of the RsmI-30S complex. **D**. Model of the RsmI dimer including the newly resolved CTD overlaid on the map and accompanied by cartoon representation of the RsmI domain organization and interaction sites between the two protomers (below). Regions absent in the final RsmI model are shaded in gray. Domains (and α helices) of the auxiliary RsmI protomer are denoted with a prime (') in this and subsequent figures.

30S complex ((**Fig. 1C**). Notably, the higher local resolution of the focused map (**Supplementary Fig. S3B,D**) allowed for confident modeling of the C1402 ribose 2'-O-linked NM6 within the RsmI SAM binding site (**Supplementary Fig. S4A**), the extensive interactions between RsmI and the 16S rRNA regions it contacts (**Supplementary Fig. S4B-D**), and the most complete structure of the RsmI dimer, to date, including the previously structurally uncharacterized CTD (**Fig. 1D**).

Overall, the structure reveals that RsmI binds to a tertiary surface on the 30S consisting of h44 and the 30S platform (**Fig.1A,C**), employing its three major domains for distinct functions: an N-terminal domain (NTD) which makes extensive contacts with 16S rRNA, a core domain which also contacts 16S rRNA and contains a Rossmann-like fold with a SAM binding motif, and methyltransferase catalytic activity, and the newly modeled CTD connected to the core domain by a short, flexible linker that mediates contacts most distant from the target nucleotide (**Fig. 1D**). Interaction of RsmI with the 30S subunit additionally distinguishes the two protomers within the dimeric structure, with one carrying the NM6 that is covalently attached to C1402 and thus anchored on h44 (which we refer to as the "catalytic" protomer) and the second ("auxiliary" protomer) in the opposite orientation with its SAM binding pocket facing away from h44 toward the solvent (**Fig. 1C**,**D**).

RsmI severely distorts h44 and positions C1402 for methylation using an array of conserved positive and aromatic residues.

C1402 is located deep in the minor groove of h44 with its ribose 2'-OH group facing toward the interior of the 30S subunit body, making the RsmI target site inaccessible in the assembled subunit. As such, we anticipated that a major rearrangement of h44 RNA would be necessary to allow access for modification by RsmI. Indeed, our structure reveals that RsmI unfolds h44, severely disrupting the top portion of the helix surrounding residue C1402 (**Fig. 2A**). The 5'-strand of h44 containing C1402 is pulled outward from its usual position to make multiple contacts with the NTD and Core domain of the catalytic protomer of RsmI. In contrast, the complementary nucleotides of the 3'-strand of h44 are no longer base paired and, without extensive interactions with RsmI, appear highly dynamic. The backbone path of these nucleotides was, however, visible using a lower resolution map of the full complex, allowing for approximate modelling of their location (**Supplementary Fig. S4E**). To unwind h44 and access C1402, RsmI surrounds the nucleotides before (C1400 and G1401) and after C1402 (C1403 to A1408) with a collection of conserved aromatic and positive residues derived exclusively from the catalytic protomer (**Fig. 2B**; **Supplementary Fig. S5** and **Table S2**). These residues form several interaction networks with the 16S rRNA nucleotides surrounding C1402 to disrupt the base stacking and base pairing interactions in which these nucleotides normally engage (**Fig. 2C-G**).

On the 5'-side of C1402, RsmI uses NTD residues D45, T46, R47, and H68 to form an interaction network surrounding C1400 and G1401 (**Fig. 2C; Supplementary Fig. S5B**). The side chain of R47 forms a salt bridge with the phosphate backbone of G1401 as well as a cation-π

interaction with the nucleobase of C1400. Adjacent to R47, T46 is positioned to form hydrogen bonds with the C1400 ring N3 and exocyclic carbonyl, while D45 appears to support positioning of R47 for its contacts with C1400 and G1401 by forming multiple interactions with its side and main chains. Despite the high conservation of R47 among RsmI orthologs (**Supplementary Fig. S5B** and **Table S2**) and its multiple contacts with the rRNA, substitution of R47 to alanine (R47A) does not significantly reduce the ability of RsmI to methylate its target *in vitro* (**Fig. 2C**). However, a double substitution of R47 and T46 (R47A/T46A), and thus disruption of their combined interactions with C1400-G1401, results in a modest (~35%) reduction in activity. Finally, H68 is positioned on the opposite side of C1400-G1401 and stacks on the G1401 nucleobase and makes a hydrogen bond with its ribose 2'OH group. Again, however, individual disruption of these interactions through substitution to alanine (H68A) does not detectably diminish RsmI activity (**Fig. 2C**). These data indicate that the network of interactions with 16S rRNA nucleotides to the 5' of C1402 does not appear essential for the ability of RsmI to access and modify its target nucleotide.

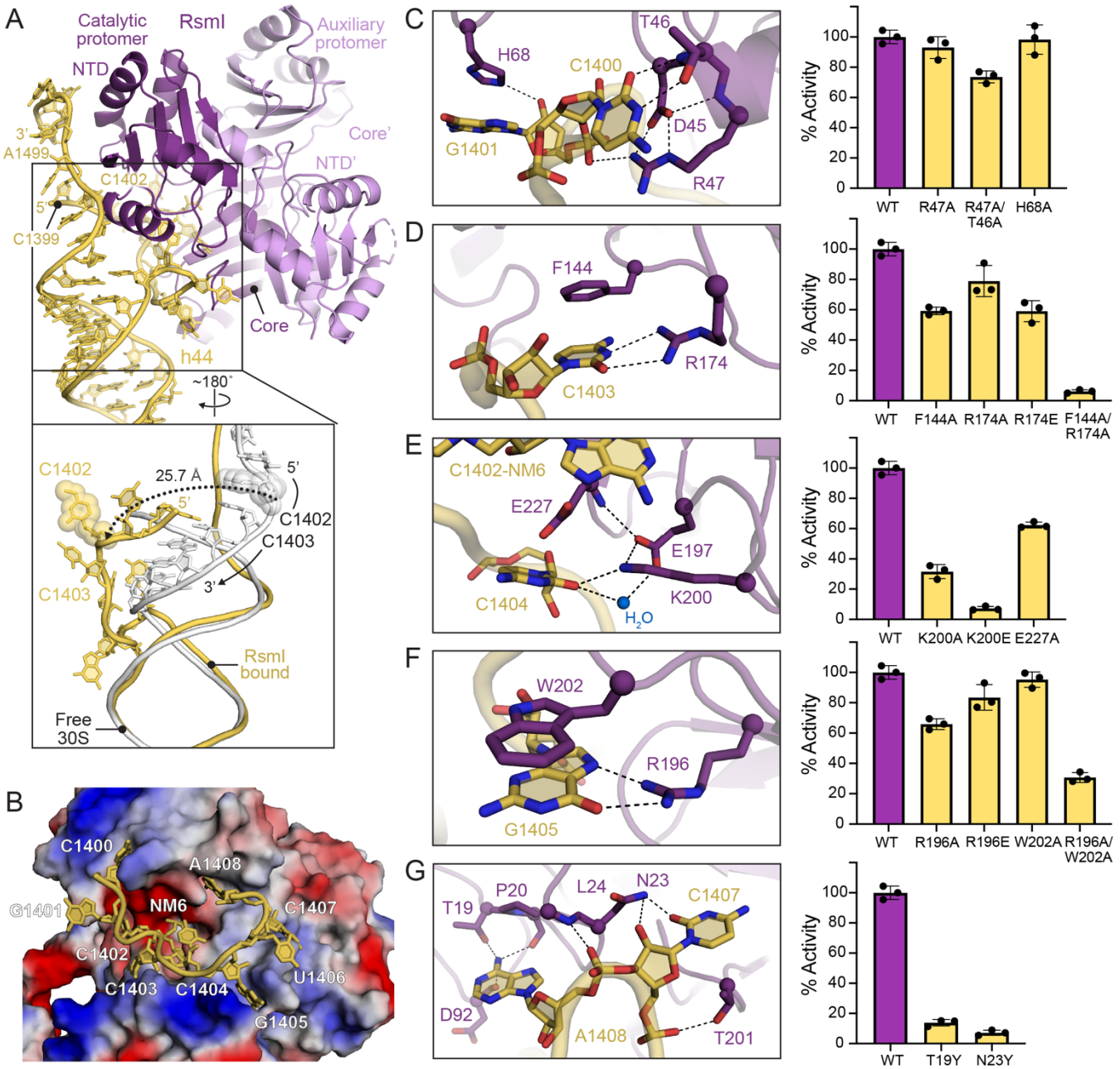

Figure 2. The RsmI catalytic protomer manipulates h44 to access target nucleotide C1402. A. View of the RsmI-h44 interface with a comparison of h44 residues C1400-A1408 between RsmI-bound (gold) and free 30S subunit (white). **B.** RsmI electrostatic surface with h44 residues C1400-A1408. Zoomed views of the interaction networks between RsmI and h44 nucleotides (*left*) and activity analyses for RsmI variants (*right*) for: **C.** C1400 and G1401, **D.** C1403, **E.** C1404, **F.** G1405, and **G.** C1407 and A1408.

In contrast, the RsmI residue interaction networks surrounding nucleotides C1403, C1404, and G1405 on the 3'-side of C1402 appear collectively crucial for the ability of RsmI to access its target nucleotide (**Fig. 2D-F**). On the immediate 3'-side of C1402, C1403 is surrounded by F144, which stacks on the nucleobase, and R174 which engages in two hydrogen bonding interactions with the Watson-Crick base edge (**Fig. 2D**). Eliminating these interactions with individual F144A or R174E substitutions both result in a similar ~40% reduction in RsmI activity, while complete disruption of this C1403

interaction network with a F144A/R174A double substitution fully ablates RsmI activity (**Fig. 2D**). At the adjacent C1404, K200 forms electrostatic interactions with both the nucleobase carbonyl oxygen and the side chain of RsmI residue E197 which, in turn, contacts the C1404 nucleobase through a water-mediated interaction (**Fig. 2E**). E197 also forms a hydrogen bond with the amide backbone of E227, which is situated in between C1404 and the adenine moiety of the NM6 covalently linked to C1402. While an E227A substitution only modestly (~40%) reduces RsmI activity, loss of the K200 positive side chain (K200A) or reversal of its charge (K200E) significantly lowers or completely eliminates RsmI activity, respectively (**Fig. 2E**). Lastly, RsmI residues R196 and W202 respectively engage in hydrogen bonding and stacking interactions with the nucleobase of G1405. While individually disrupting the interaction made by either residue by replacement with alanine (R196A or W202A) does not appreciably decrease the activity of RsmI *in vitro*, a double substitution (R196A/W202A) again has a greater impact, reducing RsmI activity by ~70% (**Fig. 2F**).

Further away from C1402 on the 3'-side, nucleotide C1407 is surrounded by RsmI residues N23 and T201. N23 engages in hydrogen bonding interactions with the C1407 nucleobase carbonyl oxygen and ribose 2'OH, while T201 forms a hydrogen bond with the phosphate backbone of C1407 (**Fig. 2G**). Immediately adjacent to C1407, nucleotide A1408 is sequestered in a pocket formed by RsmI residues T19, P20, and D92, all of which hydrogen bond with its exocyclic amine group, while the main chain amine of RsmI residue L24 forms a hydrogen bond with the A1408 phosphate group. Of the h44 nucleotides surrounding C1402 which undergo substantial RsmI-induced movement, nucleotides C1407 and A1408 are the furthest from the target nucleotide and may thus represent a site of initiation for h44 unwinding by RsmI. To assess the importance of the repositioning of these two nucleotides for subsequent access to C1402 by RsmI, we replaced N23 and T19 with bulky tyrosine residues to prevent C1407 and A1408, respectively, from moving to occupy their new positions. These N23Y and T19Y substitutions completely block the ability of RsmI to methylate C1402 (**Fig. 2G**).

Together, these data indicate that the unwinding of h44 toward C1402 depends on the coordinated movement of each nucleotide from A1408 to C1403 as disruption of the RsmI interaction network around any one of these nucleotides significantly impedes C1402 methylation (**Fig. 2D-G**). On the other hand, disruption of RsmI contact with the nucleotides 5' of C1402 (i.e., C1400 and G1401) had only minimal impact on its activity (**Fig. 2C**). Collectively, these results suggest a directionality to the unwinding of h44 by RsmI, beginning with a major repositioning of A1408 and proceeding in a 3' to 5' direction along the 5'-strand of h44 to C1402. Together, our structure and functional studies reveal that RsmI accesses C1402 by severely distorting h44 and partitioning away the residues adjacent to C1402 from their usual interactions through a redundant set of interaction networks, primarily involving conserved aromatic and positively charged residues of the catalytic RsmI protomer.

RsmI engages a conserved 16S rRNA tertiary surface to recognize its 30S subunit substrate.

RsmI requires an assembled (or late assembly intermediate) 30S subunit as its minimal substrate for C1402 modification, with its lack of activity on free 16S rRNA (7) indicating that some characteristic feature(s) only present in the mature (or near mature) 30S subunit are essential. Our structure reveals that in addition to the extensive interactions with h44, RsmI engages three additional 16S rRNA helices on the 30S subunit platform: h23b, h24a, and h45. These four 16S rRNA helices are distant in the primary sequence but are brought together in the assembled 30S subunit to form highly a conserved rRNA tertiary surface for RsmI-30S subunit interaction (**Fig. 3A, B**).

At the points of contact between RsmI and the 30S subunit platform, the rRNA tertiary surface features are structurally disrupted to varying extents by enzyme binding (**Fig. 3C-F**). At h23b, RsmI contacts nucleotides U697-A702, with minimal distortion of the RNA structure with the exception of A702, where a shift in the phosphate backbone also repositions the nucleobase 8.5 Å outward from its normal position (**Fig. 3C**). RsmI engages h24a at two separate contact points: with one strand of the helical region (nucleotides C783-G785) and with the loop at the tip of the helix (nucleotide A790) (**Fig. 3D,E**). At C783-G785 there is almost no distortion of the rRNA structure, suggesting that RsmI recognizes the h24a helical structure as a rigid unit (**Fig. 3D**). In contrast, at the tip of the helix, RsmI interaction promotes a large (8.1 Å) shift in the position of the phosphate backbone of A790 (**Fig. 3E**). Lastly at h45, RsmI contacts nucleotides G1515-G1517, inducing a modest (4.6 Å) shift in the phosphate backbone of G1517, and causing its nucleobase to rotate slightly inward toward the helix, while the position of G1515 is mostly unaffected (**Fig. 3F**). The bases of nucleotides A1518 and A1519, also rotate inward to maintain their stacking interaction with G1517. These smaller reorganizations of h45 are facilitated by the significant movement of G1516, whose nucleobase is flipped from its canonical position on the interior of the loop to an outward facing position with its nucleobase base alongside that of G1517 (**Fig. 3F**). Collectively, the distortions RsmI imposes on its rRNA binding surface appear much more widespread and substantial than has been observed to date for other 16S rRNA methyltransferases (15-17).

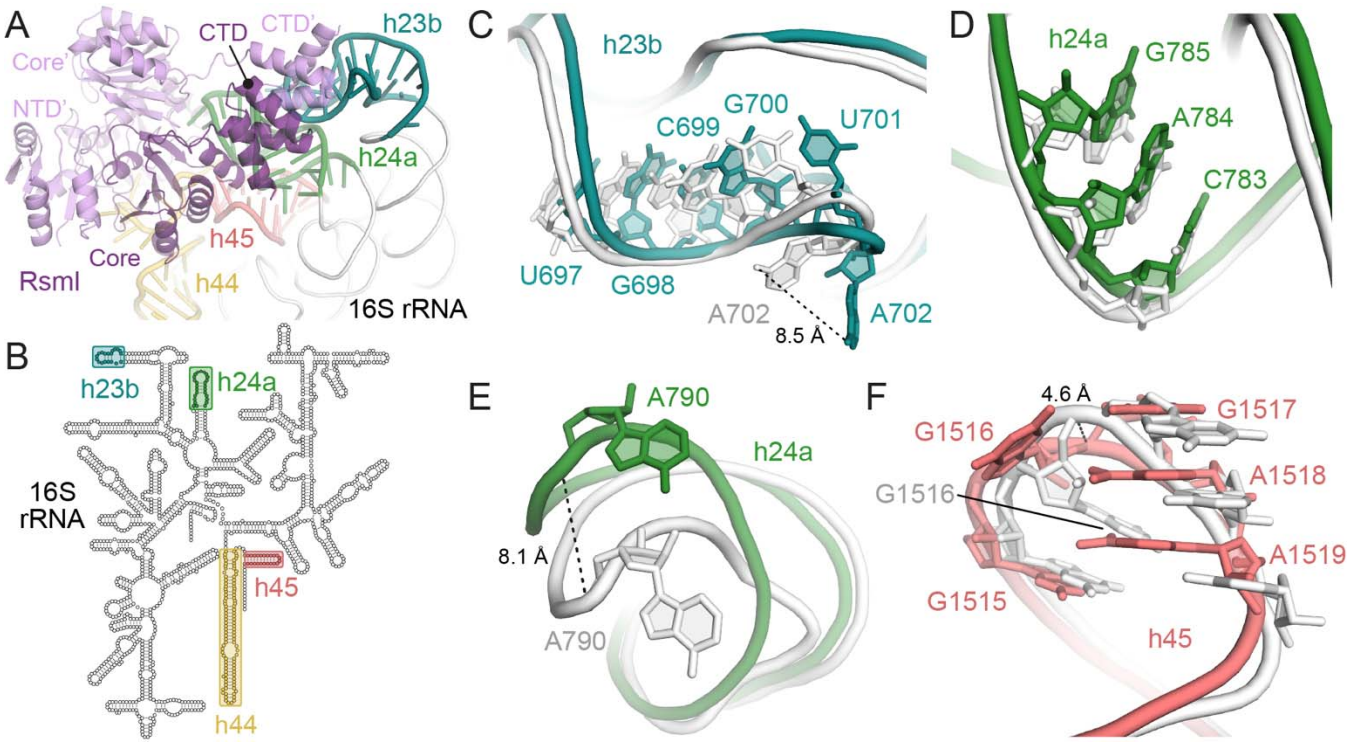

Figure 3. **RsmI binds to a 16S rRNA tertiary surface of only present in the assembled 30S subunit. A.** View of RsmI in contact with the four helices composing the 16S rRNA tertiary binding surface–h44 (yellow), h45 (red), h24a (green), and h23b (cyan). **B.** 2D representation of the 16S rRNA secondary structure, highlighting the disparate locations of the helices that compose the RsmI binding surface. Comparisons between RsmI-bound 30S subunit (colored as in panel A) and free 30S (white) at the points of contact between RsmI and **C.** h23b, **D.** h24a stem, **E.** h24a loop, and **F.** h45.

RsmI interactions with h24a and h45 are important for C1402 methylation.

In contrast to interactions with h44 which are made exclusively by the RsmI catalytic protomer, residues from both protomers of the RsmI dimer mediate the contacts with the other three helices of the rRNA tertiary surface (**Fig. 4A-D**). At h23b, RsmI engages nucleotides U697-A702 via CTD residues of its auxiliary protomer (CTD'; **Fig. 4B**; discussed further below). Surrounding h24a nucleotide A790, residues Y103 and H104 of the catalytic protomer form base stacking and hydrogen bonding interactions, respectively, with the nucleobase (**Fig. 4C**). Additionally, D137 of the auxiliary protomer forms two hydrogen bonds with the ribose 2'-OH of A790. This interaction network aligns the A790 edge with both the polar and hydrophobic groups of the modified amine group of C1402, in an enzyme-induced RNA-to-RNA interaction with the target nucleotide (**Fig. 4C**). Of the RsmI residues forming this interaction network, the aromatic nature of Y103 is the most conserved (**Supplementary Fig. S5C** and **Table S2**), suggesting that it might make the most important interaction with A790. However, a Y103A substitution alone resulted in no change in RsmI activity (**Fig. 4E**), with a modest decrease (~30-40%) only observed in combination with a second change at either the more modestly conserved H104 (to alanine) or D137 (to arginine). Further disruption of the interaction network by introduction of all three substitutions in a single variant (Y103A/H104A/D137R) did not lead to a further reduction in activity,

suggesting that loss of two interactions to A790 is sufficient to disrupt this important but not essential RsmI-30S subunit contact (**Fig. 4E**).

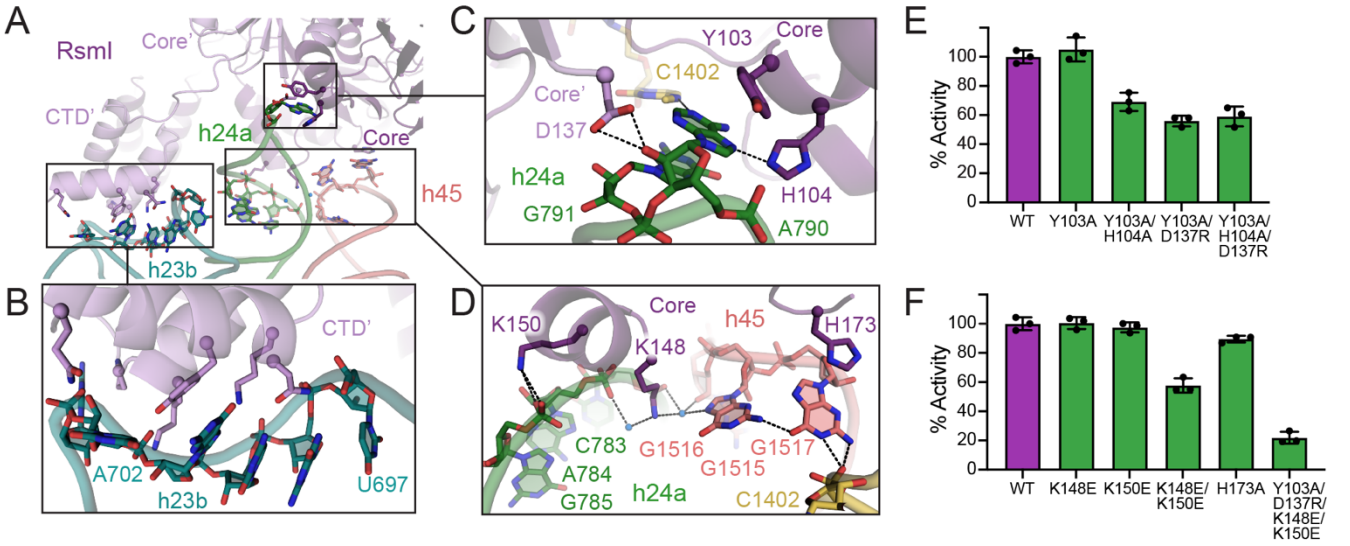

Figure 4. Functionally important contacts with the 16S rRNA surface comprising h23b, h24a and h45 are mediated by both RsmI protomers. A. Overview of the contact points between RsmI and helices h23b, h24a and h45. Zoomed in views are shown for **B.** RsmI interaction with h23b nucleotides U697-A702, mediated by the auxiliary protomer, **C.** the A790 interaction network, and **D.** h24a-h45 interface network. **E.** and **F.** Methyltransferase activity assays with variant enzymes to test the functional importance of the interaction networks shown in panels C and D, respectively.

At the second contact point on h24a (nucleotides C783-G785), RsmI residue K150 forms an electrostatic contact with the phosphate backbone between A784 and G785, while the highly conserved K148 interacts with the phosphate backbones of C783 and A784 through two water-mediated interactions (**Fig. 4D**; **Supplementary Fig. S5C** and **Table S2**). K148 also engages with the ribose 2'-OH and nucleobase N7 nitrogen of h45 nucleotides G1515 and G1516, respectively, via one of these water molecules, bridging the two 16S rRNA helices. In turn, G1516, through its flipped nucleobase, along with H173 of the RsmI catalytic protomer, interacts with G1517 through hydrogen bond and base stacking interactions, respectively. This extended interaction network connecting RsmI and the interface between h24a and h45 positions the Watson-Crick base edge of G1517 to form hydrogen bonds with the phosphate backbone of C1402, in another example of enzyme-induced RNA-to-RNA contact with the target nucleotide (**Fig. 4D**).

To assess the importance of these interactions for RsmI activity, K148 and K150 were replaced with glutamic acid both individually (K148E and K150E) and in tandem (K148E/K150E), and H173 was replaced with alanine (H173A). While no individual substitution appreciably impacted RsmI activity, the K148E/K150E double variant activity was reduced by ~40% compared to the wild-type enzyme (**Fig. 4F**). As for the RsmI interactions surrounding A790, this result suggests that the combined interactions of K148 and K150 play an important but not essential role in positioning C1402 for methylation.

Additionally, although disruption of either network individually only leads to a modest decrease in RsmI activity, their combined loss through creation of a RsmI Y103A/D137R/K148E/K150E variant led to a more drastic (~80%) reduction in activity (**Fig. 4F**), indicating that the contributions of the two interaction networks to positioning C1402 for methylation are additive.

Overall, these results reveal that RsmI forms functionally important contacts with h24a and h45 of the 16S rRNA tertiary binding surface through two distinct interaction networks. While the presence of one interaction network can help mitigate loss of the other, the combined loss of both networks–and thus more extensive disruption of contacts with h24 and h45–significantly impedes the ability of RsmI to methylate C1402. As these contacts points are distant from h44, they likely play important roles in facilitating 30S subunit recognition by RsmI as well as by directly positioning C1402 through the enzyme-induced RNA-to-RNA contacts they create with the target nucleotide.

The RsmI CTD makes functionally essential interactions with h23b.

Interaction of RsmI with h23b is exclusively mediated by the previously structurally uncharacterized CTD formed by the C-terminal 42 amino acids of the enzyme. The CTD location was clearly visible in the map for both protomers, with that of the auxiliary protomer (CTD') in direct contact with h23b (**Fig. 5A**). As this domain was missing from the published RsmI crystal structure (12) used in our initial modelling, we used AlphaFold (18) to create a preliminary structural model for the CTD, which was incorporated into the full structure for both protomers of the RsmI dimer and further refined. The newly modelled CTD consists of three α-helices (CTD-α_1, CTD-α_2, and CTD-α_3) linked to the central domain of RsmI through a short flexible linker. CTD-α_3 (residues 274–286) of the auxiliary protomer is primarily responsible for interaction of RsmI with h23b residues U697–A702. The two other helices of both protomers, CTD-α_1 (residues 244-256) and CTD-α_2 (residues 259-270), form an inter-protomer interface (**Fig. 5A**), with the catalytic protomer CTD-α_1 facing away from the 30S subunit and solvent exposed.

Previous structural and functional studies of RsmI lacking the CTD showed that the truncated enzyme can bind SAM and dimerize, but its ability to modify C1402 was not tested (12). Guided by our new structural insight, we examined the role of the CTD by creating a truncated RsmI variant lacking the last 50 amino acids (RsmI- ΔCTD). Remarkably, this truncated construct displayed virtually no ability to methylate C1402 (**Fig. 5B**), despite still containing all residues needed to manipulate h44 and interact with h24a and h45. The interactions made with h23b by CTD' of the auxiliary RsmI protomer thus appear crucial for RsmI to recognize its substrate for C1402 methylation.

Two main groups of residues contribute to the interaction between the auxiliary protomer and h23b: P258 and K260 in the loop between CTD-α_1' and CTD-α_2' and at the start of CTD-α_2', respectively, and K274, N275, Y278, and Q285 of CTD-α_3' (**Fig. 5C,D**). P258 forms a stacking interaction with A702, potentially stabilizing its observed movement, while K260 forms electrostatic

interactions with the phosphate backbone oxygens of G700 and U701 (**Fig. 5C**). Notably, both P258 and K260 are highly conserved among the Gammaproteobacteria (**Supplementary Fig. S5E** and **Table S2**). However, individual substitution of P258 with glycine (P258G) or K260 with glutamic acid (K260E) resulted in only a small reduction (~20%) in RsmI activity (**Fig. 5B**), suggesting that these interactions are not individually critical for h23b interaction.

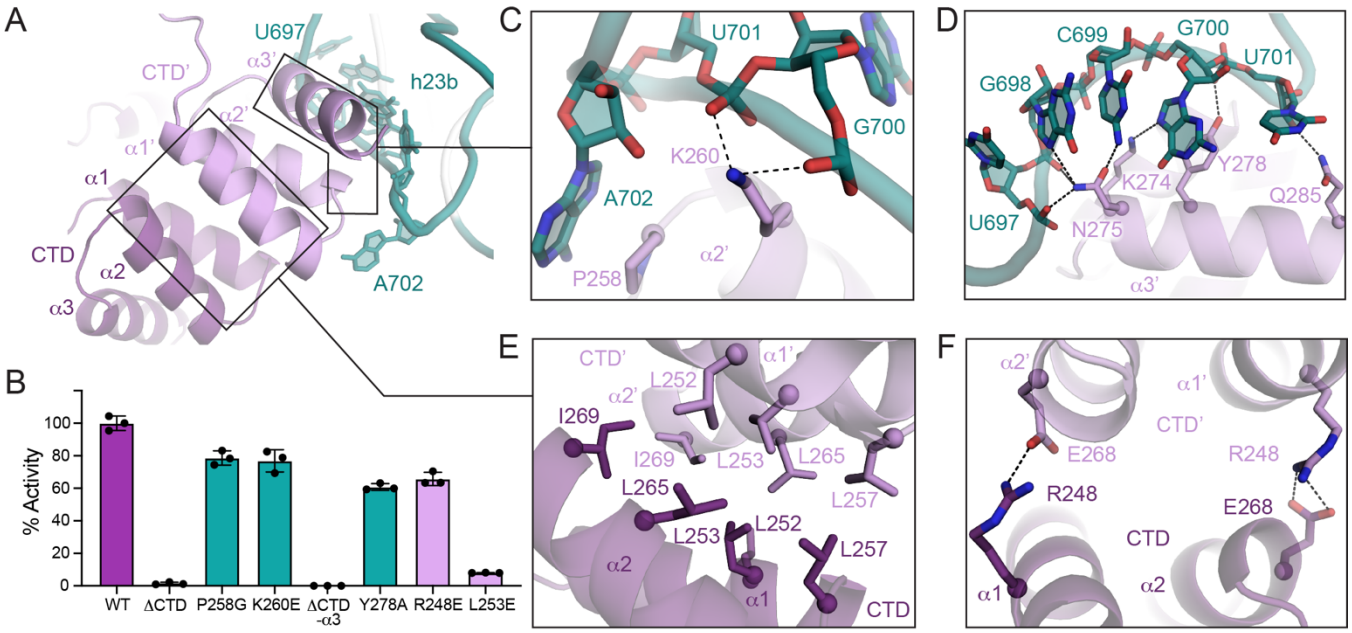

Figure 5. The RsmI CTD interaction with h23b is essential for C1402 modification. A. Structure of the CTD dimer, consisting of three α helices in each protomer: CTD-α_1 and CTD-α_2 primarily engage in interprotomer-contacts and CTD-α_3' of the auxiliary protomer interacts with h23b. **B.** Analysis of deletion and single amino acid variants of the RsmI CTD. Zoomed views of the interactions between h23b and **C**. P258 and K260, and **D.** CTD-α_3' residues K274, N275, Y278, and Q285. Zoomed views of the inter-protomer interaction via **E.** a leucine-rich hydrophobic patch and **F.** R248-mediated electrostatic contacts.

We similarly evaluated the role of the CTD-α_3 residues K274, N275, Y278, and Q285 which engage in a network of electrostatic, hydrogen bonding, and stacking interactions with the nucleobases and backbone of h23b nucleotides U697-U701 (**Fig. 5D**). The collective importance of this network was tested by constructing a truncated RsmI variant lacking CTD-α_3 (RsmI-ΔCTD-α_3). As for the RsmI-ΔCTD variant, the RsmI-Δα_3 displays almost no methylation activity (**Fig. 5B**), confirming that CTD-α_3' is the component primarily responsible for h23b binding. Although none of the four CTD-α_3 residues is fully conserved across all bacteria, Y278 has the highest sequence conservation (at 92% identity) and the other sites are typically at least partially conserved in their amino acid physicochemical property (**Supplementary Fig. S5E** and **Table S2**), suggesting that the collection of interactions with h23b is likely conserved across the enzyme family. Consistent with its higher sequence conservation and the observed stacking and hydrogen bonding interactions with G700, Y278 substitution with alanine (Y278A) resulted in a ~40% reduction in methylation activity (**Fig 5B**).

Although the CTD is not necessary for RsmI dimer formation (12), given its newly identified importance for RsmI activity we next asked whether the inter-protomer contacts mediated by CTD-α_1 and CTD-α_2 of each protomer might potentially assist in positioning CTD-α_3' of the auxiliary protomer for interaction with h23b. CTD-α_1 and CTD-α_2 of each RsmI protomer in the dimeric structure interact via a hydrophobic interface, primarily consisting of highly conserved leucine residues (**Fig. 5E**; **Supplementary Fig. S5E** and **Table S2**). Flanking this hydrophobic interface, residue R248 in each RsmI protomer forms electrostatic interactions with the side chain of E269 (**Fig. 5F**). To test the importance of this inter-protomer CTD interaction, we first substituted R248 to the oppositely charged glutamic acid (R248E) to introduce charge repulsion at two contact points within the inter-protomer binding interface, which lead to a ~40% reduction in methylation activity (**Fig. 5B**). We then substituted L253, the most conserved leucine within the hydrophobic binding interface (**Supplementary Fig. S5E** and **Table S2**), with glutamic acid (L253E) to introduce two negative charges in close proximity in the center of the hydrophobic interface, leading to a ~90% reduction in methylation (**Fig. 5B**).

Together, these results reveal the critical role of the RsmI CTD in 30S subunit recognition. The auxiliary protomer forms essential interactions with h23b distant from the modification site in h44, mediated primarily through CTD-α_3'. The CTD of the catalytic protomer also appears important as inter-protomer CTD contact mediated by CTD-α_1 and CTD-α_2, primarily through the leucine-rich hydrophobic binding interface, appears to be necessary to optimally place CTD' for h23b binding.

h44 distortion and RsmI binding-induced RNA-RNA interactions position C1402 for modification via a divalent metal ion-dependent mechanism

As noted above, RsmI binding dramatically disrupts the h44 structure to expose and reposition C1402 within the active site of RsmI for ribose 2'-OH modification (**Figs. 2** and **6A**). This movement of C1402 is further supported by RsmI binding-induced distortions of h24a and h45 which result in new RNA-RNA interactions with the target nucleotide (**Figs. 4** and **6B,C**). With these rRNA movements, the C1402 2'-OH is positioned for covalent attachment to NM6, which is bound within the RsmI SAM binding site in a manner almost identical to SAM (12), confirming that our structure using the SAM analog accurately reflects the enzyme-cosubstrate complex (**Fig. 6D**). However, our structure trapped in an intermediate post-catalytic state additionally reveals water-mediated interactions between RsmI residues E170 and E227 with the NM6 ribose and adenine moieties, respectively, that were not previously observed in the RsmI-SAM crystal structure (12) (**Fig. 6D**).

Interestingly, our structure also identified a Mg^{2+} ion coordinated by the C1402 2'-OH, C1403 phosphate backbone, and the negatively charged RsmI residues E44, D92, and D100, which are 90-100% conserved among all RsmI enzymes (**Fig. 6E; Supplementary Fig. S4D** and **Table S2**). The position of this Mg^{2+} at the modification site suggests that it might play an important role in stabilizing the ribose 2'-OH and priming it to accept the methyl group. To test this idea, we first substituted

residues E44 and D92 with alanine individually (E44A and D92A) and together (E44A/D92A). D100 was not tested as this residue was previously substituted with alanine resulting in complete disruption of SAM binding (12) and thus methyltransferase activity. While the D92A substitution did not cause a reduction in RsmI activity, the E44A and the E44A/D92A variants displayed almost complete loss of RsmI activity (**Fig. 6F**). This result implicates E44 in an essential role in Mg^{2+} coordination and as a residue critical for RsmI function.

To further probe the role of Mg^{2+} in the RsmI catalytic mechanism, we tested the activity of wild-type RsmI under varying Mg^{2+} concentrations, reducing from 10 mM used in the prior assays to the lowest concentration of 0.27 mM (corresponding to the divalent ion contributed to the reaction by the 30S subunit storage buffer). Notably, this Mg^{2+} concentration is similar to that used to split ribosomal subunits during their purification (19). Therefore, we expected the 30S subunit to retain its overall structural integrity at the lowest Mg^{2+} concentration but recognized the potential for a general destabilization of the RNA structure across the 16S rRNA surface necessary for RsmI interaction. Therefore, as a control, we performed equivalent methyltransferase assays with the 16S rRNA (m^1A1408) methyltransferase NpmA, which also requires an assembled 30S subunit to function and docks on a similar rRNA tertiary surface but only minimally disrupts its structure (15). NpmA activity declines with each reduction in Mg^{2+} concentration, consistent with this enzyme docking rigidly on a pre-formed rRNA surface which becomes increasing less stable as the divalent ion concentration is reduced. Importantly, however, even at the lowest concentration, NpmA retains about 40% activity (**Fig. 6G**). In contrast, the activity of RsmI is essentially unaffected by the reduced divalent ion concentration until a critical threshold between 1 and 0.27 mM, at which point activity is fully ablated, confirming the dependence of RsmI on the divalent ion (**Fig. 6H**). We draw two conclusions from this finding. First, RsmI activity is less sensitive to the intermediate Mg^{2+} concentrations and associated destabilization of the rRNA tertiary surface as, unlike NpmA, RsmI must distort this structure to access its target. Second, the subsequent complete loss of activity at <1 mM Mg^{2+} directly implicates this coordinated divalent metal in the RsmI catalytic mechanism. Finally, to assess whether this dependence is specific to Mg^{2+}, we replaced Mg^{2+} with Mn^{2+} at 10 mM and found that both NpmA and RsmI retained >70% activity (**Fig. 6G, H**).

Together, these analyses of RsmI variants and divalent ion concentration reveal that methylation of the C1402 2'-OH by RsmI involves a divalent metal ion-dependent catalytic mechanism. Further, RsmI uses a collection of conserved negatively charged residues to coordinate this ion, with residue E44 being essential for this function.

Discussion

The ribosomal P site in the 30S subunit contains four 16S rRNA nucleotide modifications incorporated by the intrinsic methyltransferases RsmE (m^3U1498), RsmF (m^5C1407), RsmH (m^4C1402) and RsmI (Cm1402) (7, 20, 21). These ubiquitously conserved, yet seemingly non-essential, bacterial enzymes likely function late in 30S subunit biogenesis given their shared substrate requirement for a mature or near mature 30S subunit (7, 21, 22), with their respective rRNA modifications being implicated in tuning translation (7, 23) and antibiotic susceptibility (6, 7, 23-26). However, why the 30S subunit P site retains these four methylations, how the enzymes responsible access and modify their target nucleotides, and what role(s) these methyltransferases and/or their modifications play in 30S subunit assembly have remained unclear.

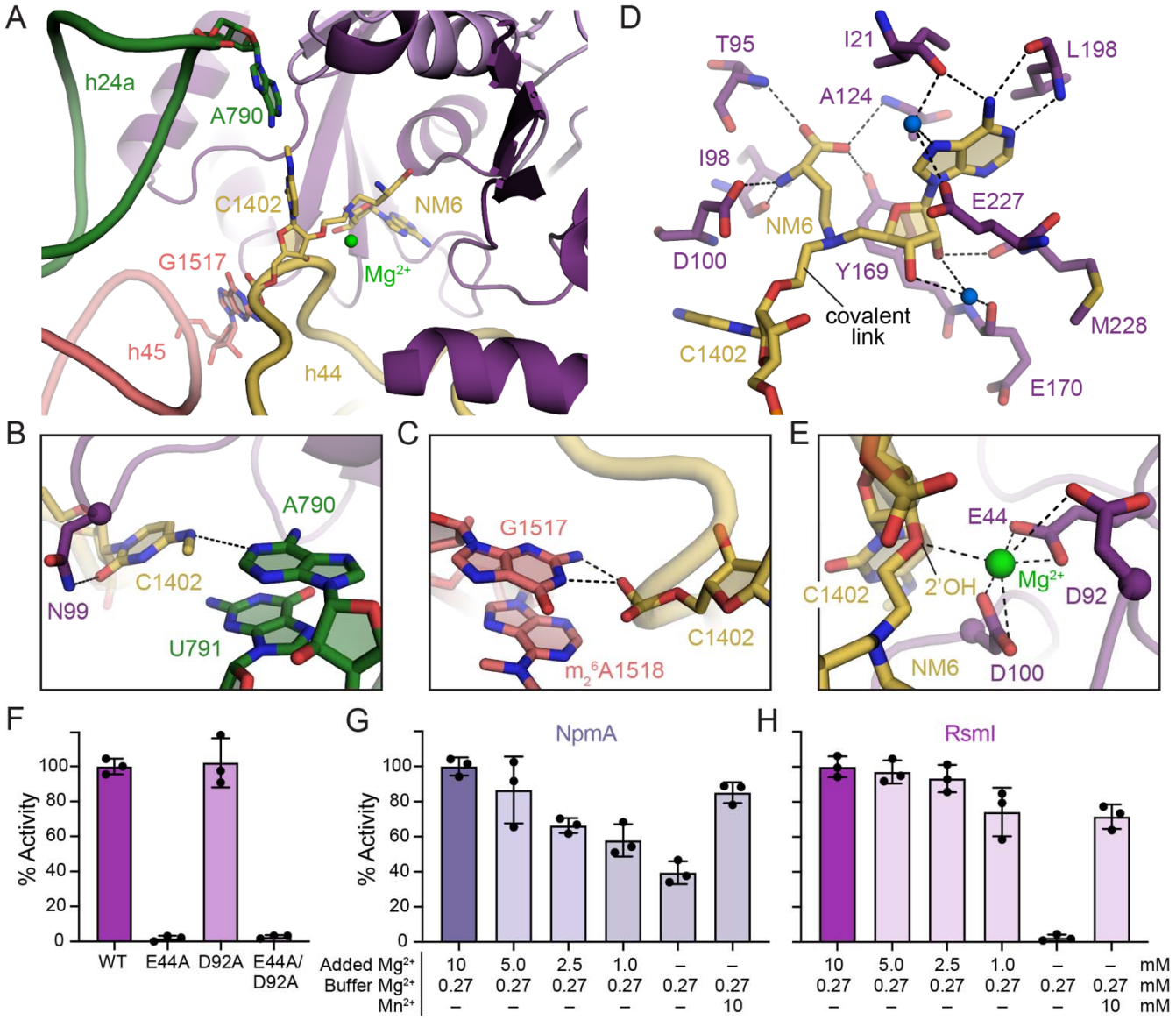

Figure 6. Catalysis of C1402 2'-O-methylation by RsmI depends on enzyme-induced RNA rearrangement and divalent metal ion. **A.** Overview of target nucleotide C1402 position between RsmI, h24, and h45. Zoomed

views of the RsmI-induced RNA-to-RNA interactions between C1402 and **B.** h24a nucleotide A790 and **C.** h45 nucleotide G1517. **D.** View of C1402 covalently bound to NM6, in the RsmI SAM-binding pocket. **E.** View of the Mg^{2+} coordination network between the C1402 2'-OH, C1403 backbone, and RsmI residues E44, D92, and D100. **F.** Functional studies of the RsmI residues coordinating the Mg^{2+}. Results of functional studies for **G.** NpmA and **H.** RsmI in which enzyme activity was tested with varying Mg^{2+} concentration or replacement of Mg^{2+} with Mn^{2+} in the reaction buffer.

To address such questions for the 2'-O-methyltransferase RsmI, we determined its mechanism of 30S subunit substrate recognition and modification using single-particle cryo-EM and complementary functional analyses. These studies revealed that RsmI accesses C1402 within the context of the assembled 30S subunit by inducing substantial distortion and unwinding of h44 via interactions mediated by the catalytic protomer of its dimeric structure. We also show that the requirement of RsmI for an assembled 30S subunit as a substrate arises from its interaction with an extended 16S rRNA tertiary surface consisting of h23b, h24a, h44, and h45. The interaction made by RsmI with h24a and h45 promote novel RNA-to-RNA contacts with the C1402 target nucleotide that are important for activity. Meanwhile, the functionally essential interaction with h23b, most distant from C1402, is mediated exclusively by the newly resolved CTD of the noncatalytic RsmI protomer, additionally revealing why RsmI functions as a dimeric enzyme. The extensive interactions made by RsmI and the resulting distortions of the 16S rRNA tertiary surface collectively reposition the ribose 2'-OH of C1402 to receive a methyl group from the SAM co-substrate in a divalent metal-ion dependent process.

The unraveling of h44 by RsmI represents the most severe distortion of the 16S rRNA structure by a 30S subunit-targeting rRNA methyltransferase observed to date (15-17). How RsmI is able to induce such a major structural distortion in h44, including disruption of multiple base pairs in the absence of energy-driven helicase activity, can be rationalized by our structure-guided functional analyses of the key interaction clusters at h44. These data suggest that RsmI begins the process of unravelling h44 via its interactions with A1408, several nucleotides distant from the site of modification, and then employs an array of conserved positive and aromatic residues to unpair the RNA duplex of h44 in a 3' to 5' direction, culminating in a ~26 Å movement of C1402 from its normal position within h44 into the RsmI catalytic center. A1408 is not involved in a canonical Watson-Crick base pair within h44 as it is located opposite two dynamic nucleotides, A1492 and A1493, that unstack from the helix interior as part of their essential role in probing mRNA-tRNA interaction during decoding (27). This increases the mobility of the A1408 nucleobase, a feature that has been proposed to be exploited by the aminoglycoside-resistance m^1A1408 methyltransferase NpmA which rigidly docks on the 30S subunit to capture A1408 between two conserved Trp residues when flipped from h44 (15). Unlike RsmI, the movement of A1408 is the only disruption of the 16S rRNA structure observed when NpmA is bound to its 30S substrate. Our data suggest that RsmI also exploits this dynamic nature of A1408 to gain an initial anchor point for h44 unwinding as blocking the movement of A1408 eliminates

modification of C1402 (**Fig. 2G**). Further, supporting the idea of sequential unwinding from A1408 to C1402, the interaction networks that reposition nucleotides between these sites are also important for efficient modification, whereas interactions observed to the 5' side of C1402 appear to be essentially dispensable.

The requirement of a structurally conserved 16S rRNA tertiary binding surface on the 30S subunit is a feature RsmI shares with several other 16S rRNA methyltransferases studied to date, including NpmA (16), the aminoglycoside-resistance m^7G1405 methyltransferase RmtC (16), and the universally conserved intrinsic $m_2^{6,6}$A1518/ $m_2^{6,6}$A1519 dimethyltransferase RsmA (formerly KsgA) (17). However, RsmI appears distinct in the extent of its 16S rRNA interaction surface, with contacts made to h44 and h23b that span a distance of >70 Å and bury an interface of over 3000 $Å^2$, more than 2.5× that buried by NpmA (15). Recognition of the distant h23b is essential for RsmI to modify C1402 as loss of these contacts made by the auxiliary protomer fully eliminate enzyme activity. A further distinction is that the three other 16S rRNA methyltransferases appear to use the 16S rRNA tertiary surface as rigid docking platforms, with rRNA structural deformations restricted to regions immediately surrounding their target sites in h44 (NpmA and RmtC) or h45 (RsmA) (15-17). In contrast, in addition to major disruption of h44, RsmI engagement with h24a and h45 results in additional structural distortions of the rRNA more distant from the target site. Further, these reorganizations of the rRNA structure promote new enzyme-induced RNA-to-RNA contacts with the target nucleotide, potentially assisting in stabilizing C1402 for modification. Thus, RsmI appears to engage and manipulate the 16S rRNA tertiary surface in three distinct ways to achieve specific substrate recognition and access C1402 for modification: rigid docking at a distant conserved structural feature (h23b), extensive disruption of h44, and distortion of other 16S rRNA helices (h24a and h45) to assist in positioning C1402. Whether the other intrinsic 16S rRNA methyltransferases acting in the P site (RsmE, RsmF and RsmH) employ similar molecular strategies to access their targets will require corresponding studies of their 30S-enzyme complexes. Given its shared target nucleotide with RsmI, the 30S-RsmH complex would be particularly informative on the potential diversity in molecular recognition strategies used by these enzymes.

This work also revealed that RsmI unexpectedly depends on a divalent metal ion for catalysis of C1402 ribose 2'OH methylation. The well-studied and essential bacterial m^1G37 tRNA methyltransferase TrmD similarly requires a divalent metal ion which is thought to increase the nucleophilicity of the N1 position and stabilize the developing negative charge on O6 during methyl transfer (28). Like TrmD, RsmI surrounds the divalent metal ion with a collection of negatively charged amino acids to help chelate the ion. However, in contrast to TrmD, where metal coordination is completed by the carboxylic tail of SAM and, presumably, by the nitrogen base of its substrate G37 (29), metal coordination in the RsmI-30S complex is completed by the C1403 phosphate backbone and C1402 2'-OH group without interaction with the cosubstrate. While to our knowledge RsmI represents

the first characterized example of a metal-dependent RNA ribose 2'-OH methyltransferase, direct involvement of the target oxygen atom in metal coordination may be a feature shared across other metal-dependent O-methyltransferases as it is also present among metal-dependent catechol and flavonoid O-methyltransferases (30-32). For example, RsmI and the alfalfa caffeoyl coenzyme A 3-*O*-methyltransferase share strikingly similar metal coordination arrangements despite their distinct substrates. In this enzyme, the metal ion is proposed to deprotonate its target hydroxyl group and maintain the resulting oxyanion near SAM's reactive methyl group (31). Given the similarities in metal ion coordination, RsmI may similarly use the bound divalent metal during catalysis. As both an RNA-modifying and metal-dependent O-methyltransferase, RsmI may represent the first of a unique subclass of SAM-dependent RNA methyltransferases.

Chemical modification processes of the bacterial small subunit have been proposed to serve as quality control check points in 30S subunit assembly. For example, binding and 16S rRNA modification by RsmA has been suggested to act as a final checkpoint for the integrity of 30S platform assembly while also allowing time for completion of other late-stage 30S assembly processes (2, 17, 33). The action of RsmI late in 30S assembly and the manner in which it engages and manipulates the folded 16S rRNA suggest potential for roles similar to RsmA in 30S subunit biogenesis and quality control. For instance, coordinated recognition of distant sites (h44 and h23b) implicates RsmI as quality control factor for both the correct folding of the 30S platform and the placement of h44 in relation to a properly folded platform, the absence of which could stall RsmI action. Additionally, the extensive unfolding of h44 comprising a key functional region of the ribosome offers a potential "reset button" and opportunity for correct refolding of the ribosomal P site and adjacent decoding center. This idea is further reinforced by our results showing that RsmI can withstand destabilization of the 30S surface during C1402 modification (**Fig. 6H**). Further, given the overlapping binding sites of RsmI with either mRNA, translation initiation factor 3, or H69 of the 50S subunit in the context of a functional 70S (34, 35), the presence of RsmI on pre-mature 30S subunits could also serve to impede binding of other factors, effectively removing the 30S subunit intermediates from participating in translation. Thus, the full functional importance of RsmI, RsmA and potentially other intrinsic 16S rRNA methyltransferases may not derive exclusively in the direct effects of the methyl groups they deposit, but also through the mechanisms by which they recognize and manipulate the pre-mature 30S subunit during the modification process.

Our structure-guided approach to deciphering RsmI's mechanism of action has expanded our understanding of the breadth of rRNA methyltransferase action in terms of 30S subunit recognition, rRNA manipulation and metal ion coordination in catalysis of rRNA modification. Moreover, our studies provide further support for the concept of intrinsic bacterial methyltransferases as ribosome assembly

checkpoints, helping to contextualize how we view such intrinsic bacterial methyltransferases beyond just depositors of methyl modifications.

Materials and Methods

Generation of an E. coli ΔrsmI strain for 30S subunit isolation–An *E. coli* strain lacking RsmI activity was generated by replacing *rsmI* with a chloramphenicol acetyltransferase gene (*cat*) using conventional gene replacement strategies (7, 36) (**Supplementary Fig. S1A**). *cat* and its promoter were amplified from the plasmid pZS21 (37, 38) using primers to incorporate 40 nucleotide extensions homologous to *rsmI* at each end (**Supplementary Table S3**). The resulting *cat* cassette was used to transform via electroporation *E. coli* strain DY378, which endogenously expresses the lambda red homologous recombination machinery under temperature control (39). Finally, P1 phage transduction (40), was used to transfer the Δ*rsmI* genotype to *E. coli* BW25113 (36). Replacement of *rsmI* with *cat* was verified through PCR amplification of genomic DNA extracted using the DNeasy Blood and Tissue Kit (Qiagen) (**Supplementary Fig. S1B** and **Table S3**). Wild-type BW25113 and 30S-Δ*rsmI* ribosomal subunits were prepared by iterative rounds of high-speed centrifugation to isolate the ribosomal fractions of the cell followed by sucrose gradient centrifugation at low Mg^{2+} concentration to separate the 30S subunit from the rest of ribosomal populations, as done previously (41). Δ*rsmI* 30S were shown to be unmethylated at C1402 (and thus a substrate for RsmI) using an *in vitro* methylation assay (**Supplementary Fig. S1C,D**).

RsmI protein expression, purification and site-directed mutagenesis–The sequence encoding RsmI was amplified from *E. coli* BW25113 genomic DNA (**Supplementary Table S3**) and subcloned into a pET44a vector with an N-terminal hexahistidine tag (pET44-RsmI). This plasmid was used to transform *E. coli* BL21(DE3) cells with subsequent growth at 37˚C in lysogeny broth containing ampicillin (100 µg/ml). Protein expression was induced at mid-log phase (~0.6 OD_{260}) with 1 mM isopropyl β-D-1-thiogalactopyranoside and growth continued for another 3 hours before being harvested via centrifugation at 4˚C. Cells were resuspended in lysis buffer (50 mM HEPES-NaOH, pH 7.6, 1 M NaCl, 10 mM imidazole, 0.5% Triton X-100, and 2 mM β-mercaptoethanol containing the protease inhibitors PMSF and benzamidine) and lysed by sonication (Misonix Sonicator 3000 with microtip: 7.5-min total sonication time, 1-s on, 1-s off, output level 5.0). Cell lysates were cleared by centrifugation at 4˚C and then dialyzed three times (2 x 3 hours and overnight) against a high salt buffer (50 mM HEPES-NaOH, pH 7.6, 2 M NaCl, 10 mM imidazole, and 2 mM mM β-mercaptoethanol) to remove any SAM copurifying with RsmI. The lysate was then dialyzed for 3 hours against the same buffer but with reduced salt (500 mM NaCl) and applied to a Cytiva HisTrap FF crude 1 mL column on an ÄKTA Purifier 10 System equilibrated in the same buffer. The column was washed for 15 column

volumes with the same buffer but containing 25 mM imidazole and protein subsequently eluted by increasing imidazole to 500 mM. The eluted protein sample was further purified using a Superdex75 16/60 gel filtration column (Cytiva) equilibrated in gel filtration buffer (10 mM HEPES-NaOH, pH 7.6, 300 mM NaCl, and 2 mM β-mercaptoethanol).

RsmI variants were generated in the pET44-RsmI plasmid using the MEGAWHOP mutagenesis method (42). Primers used for first round PCR (to generate the "mega" primers) are listed in **Supplementary Table S3**. All RsmI variant proteins were expressed as for the wild-type protein. A simplified purification strategy was used for wild-type and variant RsmI proteins for use in functional assays, using NEBExpress Ni Spin Column for affinity purification with minor modifications: three wash steps were done with increasing imidazole concentrations of 25, 50, and 100 mM before elution with 500 mM imidazole. Protein folding/ stability and prep-to-prep quality control was done using nano differential scanning fluorimetry on a NanoTemper Tycho NT.6.

Cryo-EM specimen preparation and data collection–A 3 µl mixture of wildtype RsmI (1.2 µM), 30S-Δ*rsmI* (0.4 µM), and SAM analog NM6 (24 µM), prepared as previously described (13), was applied to glow-discharged C-flat 1.2/1.3 Au 50 300 mesh grids. Grids were blotted at 4˚C for 5 seconds at 100% humidity and frozen in liquid ethane using a Vitrobot Mark IV (Thermofisher). Cryo-EM data (8,164 micrographs) were recorded as movies with a defocus range from -0.4 to -2.9 µm at 105,000× nominal magnification (0.41 Å/pixel) on a Titan Krios 300 kV (TEM) with a Gatan K3 direct electron detector at the National Center for CryoEM Access and Training (NCCAT). Movies were collected at a dose rate of 27.37 $e^-/Å^2/s$ with a total exposure of 1.8 seconds, for an accumulated dose of 49.27 $e^-/Å^2$. Intermediate frames were recorded every 0.05 seconds for a total of 40 frames per micrograph.

All image processing steps were conducted in CryoSPARC (43) following the workflow outlined in **Supplementary Fig. S2**. Movies were dose-weighed and corrected for motion drift using Patch Motion Correction with the output micrographs down sampled by a binning factor of 0.5. The contrast transfer function (CTF) was estimated using Patch CTF Estimation, and images with a CTF fit resolution > 5 Å were discarded (**Supplementary Fig. S2A**). Automatic blob picking selected 3,781,314 particles, which then underwent particle picking followed by extraction with a box size of 448 pixels, down-sampled to 120 pixels for faster initial particle curation, culminating in 2,140,666 particles (**Supplementary Fig. S2B**). Using a series of 2D classifications followed by iterative rounds of *ab initio* Reconstruction and Heterogenous Refinement, only particles corresponding to 30S subunits with high RsmI occupancy were retained (356,021 particles) (**Supplementary Fig. S2B**). These particles were re-extracted at a box size of 448 pixels and underwent iterative rounds of Homogenous Refinement, Global CTF Refinement, Local CTF Refinement, and Reference Based Motion Correction to produce a final map of the complex at 2.12 Å (**Supplementary Fig. S2C**). Further particle curation through iterative rounds of 3D Classification using a mask around the enzyme and accompanied by

Heterogenous Refinement resulted in a decreased particle count of 264,656 particles, which formed a consensus 2.19 Å map after Homogenous Refinement. (**Supplementary Fig. S2D**). From this map, two separate strategies were employed. First, the particle density around RsmI and its 30S binding interface was subtracted and RsmI and its 30S contact surface locally refined using masked local refinement, leading to a 2.55 Å focused map (**Supplementary Fig. S2E**). For the second strategy, remnant 30S head-induced heterogeneity was removed and RsmI occupancy further improved through successive 3D classifications at low (16 Å) and high (6 Å) filter resolution, resulting in a final particle count of 74,553 particles. These particles underwent homogenous refinement followed by masked local refinement without particle subtraction, resulting in a 2.42 Å map of the entire complex (**Supplementary Fig. S2F**). All masks were created using a combination of ChimeraX (44) and CryoSPARC (43). Local resolution estimates of both maps were generated using CryoSPARC (43) and visualized with ChimeraX (44) (**Supplementary Fig. S3**). Sharpened maps used for **Fig. 1** and **Supplementary Fig. S3** were generated using DeepEMhancer (45).

RsmI-30S subunit complex model building and refinement–The 2.55 Å focused map displayed better map quality for RsmI and its 16S rRNA interface, while the 2.42 Å map of the full complex displayed better quality for the rest of the 30S body. Both maps were therefore used for model building and refinement. An empty 30S subunit structure (PDB 7OE1) (46) and the RsmI NTD and core domains from the RsmI-SAM complex crystal structure (PDB 5HW4) (12) were rigid-body fitted into both maps using ChimeraX (44) to create a starting model. After initial real-space refinement with global minimization, simulated annealing, local grid search, and ADP-factor refinement against the full map in Phenix 1.21-5207 (47), the model was truncated to the regions within the focused map (both RsmI protomers and 16S rRNA nucleotides 682-708, 780-802,1399-1413,1486-1494, and 1507-1527) and further refined against the focused map using Phenix (47) (***Supplementary*** **Table S1)**. Residues of h44 interacting with RsmI were substantially reorganized compared to their normal locations in the 30S subunit and were manually re-built in Coot 0.9.8.95 (48) with real space refinement. Additionally, Coot (48) was used to *de novo* model the NM6-modified C1402 residue and to make all other necessary adjustments of residues for optimal fit in the map. The refined truncated region was then combined with the rest of the model, which underwent additional rounds of Phenix (47) real-space refinement with global minimization and ADP refinement coupled with geometry minimization and manual model adjustment in Coot (48), using both maps to refine distinct parts of the model. Inherent movement of the 30S head domain resulted in poorer map quality for this region and limited our ability to accurately model the corresponding 16S rRNA residues and associated ribosomal proteins. Additionally, two highly flexible residues (1397 and 1398) which link h44 to the 30S head were not included in the model. Residues 1494-1506 also displayed disorder but could be modeled and refined using a low-resolution version of the full map which showed visible density for this region (**Supplementary Fig. S4E**).

A model of the 7-amino acid linker and 42-amino acid CTD was generated using the AlphaFold 3 Server (18). Two copies of this model, one for each RsmI protomer, were then rigid-body fitted into available density on the 2.55 Å focused map using ChimeraX (44) and refined using Phenix (47). The additional domains were then covalently linked to the initial RsmI (NTD-core) structure using a combination of PyMOL (49) and Coot (48). The contacts between RsmI and the 30S platform were then further refined using Phenix (47) with finer adjustments made in Coot (48), as before. Water and Mg^{2+} were added manually using Coot (48).

The final model was validated in Phenix (47), and the coordinates and both maps deposited in the Protein Data Bank (accession code 9PZG) and Electron Microscopy Database (accession code EMD-72071)**.** All parameters pertaining to data collection, image processing, model building and refinement, and model validation are summarized in ***Supplementary*** **Table S1**. Structural alignments were performed and solvent exposed surface area was calculated in PyMol, the latter using the get_area command with default 1.4 Å probe radius. Figures showing maps and structural images were generated using PyMOL (49) or ChimeraX (44).

RsmI conservation analysis–RsmI methyltransferase sequences were retrieved from UniProt using the InterPro identifier IPR018063. Sequence redundancy was removed by applying a 90% sequence identity cutoff (UniRef90) and clusters with fewer than 50 sequences were excluded. This process yielded a final set of 198 representative RsmI sequences, covering all major bacterial groups including Proteobacteria (Alpha-, Beta-, Gamma-, and others), Firmicutes, Actinobacteria, Cyanobacteria, and thermophilic bacteria. Multiple sequence alignment was performed in Geneious, and a neighbor-joining phylogenetic tree was generated to identify and isolate the Gammaproteobacterial RsmI clade. Residue propensities were calculated and sequence logos generated in Geneious software.

[^{3}H]-SAM methyltransferase assay–Methylation of 30S subunit by wild-type and variant RsmI proteins was quantified using a filter-based enzyme assay with [^{3}H]-SAM. In initial assays to test RsmI activity on the 30S-Δ*rsmI* subunit, wild-type RsmI (0.4 µM) was incubated with [^{3}H]-SAM (0.84 µM) and either wild-type 30S or 30S-Δ*rsmI* subunit (0.4 µM) in Buffer G (5 mM HEPES-KOH, pH 7.5, 50 mM KCl, 10 mM NH_4Cl, 10 mM magnesium acetate, and 6 mM β-mercaptoethanol) in a final reaction volume of 10 µl. The reaction was incubated for 90 minutes at 37˚C and then quenched with 90 µl of ice-cold 5% trichloroacetic acid (TCA). The quenched reaction was transferred to a glass microfiber filter, which was washed 3× with 200 µl 5% TCA and 2× with 200 µl 70% ethanol. After drying overnight, ^{3}H retained on the filter (i.e., extent of 30S methylation) was determined by scintillation counting using a Beckman Coulter LS6500 liquid scintillation. A control assay with no added enzyme was used to determine background values which were then subtracted from the experimental counts.

To establish optimal conditions for comparisons between variant RsmI enzymes, a time-course experiment was conducted with wild-type RsmI (0.1 µM), [^{3}H]-SAM (0.84 µM), and 30S-Δ*rsmI* (0.1 µM) in Buffer G in a total volume of 90 µl. The reaction was incubated for 120 minutes at 37 ˚C, with 10 µl aliquots removed and quenched with 90 µl 5% TCA at 0, 5, 10, 20, 40, 60, 90, and 120 minutes. Subsequent steps and data analysis were performed as described above (**Supplementary Fig. S1D**). A single 20-minute time point where wild-type RsmI reaches 80-90% of maximum methylation was subsequently selected for the analyses of all RsmI variants performed under otherwise identical conditions. All assays with RsmI variants were performed alongside similarly purified wild-type RsmI and with background control. All methylation assay data were plotted in GraphPad Prism 10 following normalization to values for wild-type RsmI.

Finally, methylation assays with varying divalent ion (Mg^{2+} or Mn^{2+}) concentrations were conducted essentially identically other than variations in Buffer G to alter the final added magnesium acetate (0 to 10 mM) or $MnCl_2$ concentrations. All assays additionally contained 0.27 mM magnesium acetate from the 30S subunit storage buffer.

Data Availability

Cryo-EM maps and atomic models have been deposited in the Electron Microscopy Databank (EMD-72071) and Protein Databank (PDB ID: 9PZG), respectively. All other data are included in the manuscript and/or supporting information.

Acknowledgements

This study was supported by the National Institutes of Health awards R01 AI088025 (to G.L.C. and C.M.D.), T32 GM135060 (to M.I.B.) and F31 AI186518 (to M.I.B.). C.M.D. is a Burroughs Wellcome Fund Investigator in the Pathogenesis of Infectious Disease recipient. This study was also supported by the Robert P. Apkarian Integrated Electron Microscopy Core (IEMC) at Emory University, which is subsidized by the Emory School of Medicine and Emory College of Arts and Sciences. Some of this work was performed at the National Center for CryoEM Access and Training (NCCAT) and the Simons Electron Microscopy Center located at the New York Structural Biology Center, supported by the NIH Common Fund Transformative High Resolution Cryo-Electron Microscopy program (U24 GM129539, and NIGMS R24 GM154192) and by grants from the Simons Foundation (SF349247) and NY State Assembly. We would like to thank Dr. Marcin Grabowicz for advice on generating the Δ*rsmI* strain and providing the *E. coli* DY378 strain and pZS21 plasmid.

References

1. W. A. Decatur, M. J. Fournier, rRNA modifications and ribosome function. *Trends Biochem Sci* **27**, 344-351 (2002).

2. K. Connolly, J. P. Rife, G. Culver, Mechanistic insight into the ribosome biogenesis functions of the ancient protein KsgA. *Mol Microbiol* **70**, 1062-1075 (2008).

3. K. Connolly, G. Culver, Overexpression of RbfA in the absence of the KsgA checkpoint results in impaired translation initiation. *Mol Microbiol* **87**, 968-981 (2013).

4. Y. S. Polikanov, S. V. Melnikov, D. Soll, T. A. Steitz, Structural insights into the role of rRNA modifications in protein synthesis and ribosome assembly. *Nat Struct Mol Biol* **22**, 342-344 (2015).

5. D. E. Burakovsky *et al.*, Impact of methylations of m2G966/m5C967 in 16S rRNA on bacterial fitness and translation initiation. *Nucleic Acids Res* **40**, 7885-7895 (2012).

6. A. Babosan *et al.*, Nonessential tRNA and rRNA modifications impact the bacterial response to sub-MIC antibiotic stress. *Microlife* **3**, uqac019 (2022).

7. S. Kimura, T. Suzuki, Fine-tuning of the ribosomal decoding center by conserved methyl-modifications in the Escherichia coli 16S rRNA. *Nucleic Acids Res* **38**, 1341-1352 (2010).

8. A. Vila-Sanjurjo, A. E. Dahlberg, Mutational analysis of the conserved bases C1402 and A1500 in the center of the decoding domain of Escherichia coli 16 S rRNA reveals an important tertiary interaction. *J Mol Biol* **308**, 457-463 (2001).

9. J. Rinke-Appel *et al.*, Site-directed cross-linking of mRNA analogues to 16S ribosomal RNA; a complete scan of cross-links from all positions between '+1' and '+16' on the mRNA, downstream from the decoding site. *Nucleic Acids Res* **21**, 2853-2859 (1993).

10. A. Delgado-Tejedor *et al.*, Native RNA nanopore sequencing reveals antibiotic-induced loss of rRNA modifications in the A- and P-sites. *Nat Commun* **15**, 10054 (2024).

11. T. Kyuma *et al.*, Ribosomal RNA methyltransferases contribute to Staphylococcus aureus virulence. *FEBS J* **282**, 2570-2584 (2015).

12. M. Zhao *et al.*, Structural insights into the methylation of C1402 in 16S rRNA by methyltransferase RsmI. *PLoS ONE* **11**, e0163816 (2016).

13. R. L. Weller, S. R. Rajski, Design, synthesis, and preliminary biological evaluation of a DNA methyltransferase-directed alkylating agent. *Chembiochem* **7**, 243-245 (2006).

14. V. Stanevich *et al.*, The structural basis for tight control of PP2A methylation and function by LCMT-1. *Mol Cell* **41**, 331-342 (2011).

15. J. A. Dunkle *et al.*, Molecular recognition and modification of the 30S ribosome by the aminoglycoside-resistance methyltransferase NpmA. *Proc Natl Acad Sci U S A* **111**, 6275-6280 (2014).

16. P. Srinivas *et al.*, 30S subunit recognition and G1405 modification by the aminoglycoside-resistance 16S ribosomal RNA methyltransferase RmtC. *Proc Natl Acad Sci U S A* **120**, e2304128120 (2023).

17. N. C. Stephan, A. B. Ries, D. Boehringer, N. Ban, Structural basis of successive adenosine modifications by the conserved ribosomal methyltransferase KsgA. *Nucleic Acids Res* **49**, 6389-6398 (2021).

18. J. Abramson *et al.*, Accurate structure prediction of biomolecular interactions with AlphaFold 3. *Nature* **630**, 493-500 (2024).

19. S. J. Hardy, C. G. Kurland, P. Voynow, G. Mora, The ribosomal proteins of Escherichia coli. I. Purification of the 30S ribosomal proteins. *Biochemistry* **8**, 2897-2905 (1969).

20. G. N. Basturea, K. E. Rudd, M. P. Deutscher, Identification and characterization of RsmE, the founding member of a new RNA base methyltransferase family. *RNA* **12**, 426-434 (2006).

21. N. M. Andersen, S. Douthwaite, YebU is a m5C methyltransferase specific for 16 S rRNA nucleotide 1407. *J Mol Biol* **359**, 777-786 (2006).

22. G. N. Basturea, M. P. Deutscher, Substrate specificity and properties of the Escherichia coli 16S rRNA methyltransferase, RsmE. *RNA* **13**, 1969-1976 (2007).

23. P. Pletnev *et al.*, Comprehensive Functional Analysis of Escherichia coli Ribosomal RNA Methyltransferases. *Front Genet* **11**, 97 (2020).

24. A. Liu *et al.*, Antibiotic sensitivity profiles determined with an Escherichia coli gene knockout collection: generating an antibiotic bar code. *Antimicrob Agents Chemother* **54**, 1393-1403 (2010).

25. S. Bijpuria, R. Sharma, B. Taneja, Loss of U1498 methylation in 16S rRNA by RsmE methyltransferase associates its role with aminoglycoside resistance in mycobacteria. *J Glob Antimicrob Resist* **23**, 359-369 (2020).

26. B. Gutierrez *et al.*, Fitness cost and interference of Arm/Rmt aminoglycoside resistance with the RsmF housekeeping methyltransferases. *Antimicrob Agents Chemother* **56**, 2335-2341 (2012).

27. A. P. Carter *et al.*, Functional insights from the structure of the 30S ribosomal subunit and its interactions with antibiotics. *Nature* **407**, 340-348 (2000).

28. R. Sakaguchi, G. Lahoud, T. Christian, H. Gamper, Y. M. Hou, A divalent metal ion-dependent N(1)-methyl transfer to G37-tRNA. *Chem Biol* **21**, 1351-1360 (2014).

29. J. Jaroensuk *et al.*, Crystal structure and catalytic mechanism of the essential m(1)G37 tRNA methyltransferase TrmD from Pseudomonas aeruginosa. *RNA* **25**, 1481-1496 (2019).

30. J. Vidgren, L. A. Svensson, A. Liljas, Crystal structure of catechol O-methyltransferase. *Nature* **368**, 354-358 (1994).

31. J. L. Ferrer, C. Zubieta, R. A. Dixon, J. P. Noel, Crystal structures of alfalfa caffeoyl coenzyme A 3-O-methyltransferase. *Plant Physiol* **137**, 1009-1017 (2005).

32. J. G. Kopycki *et al.*, Biochemical and structural analysis of substrate promiscuity in plant Mg2+-dependent O-methyltransferases. *J Mol Biol* **378**, 154-164 (2008).

33. D. Boehringer, H. C. O'Farrell, J. P. Rife, N. Ban, Structural insights into methyltransferase KsgA function in 30S ribosomal subunit biogenesis. *J Biol Chem* **287**, 10453-10459 (2012).

34. J. P. McCutcheon *et al.*, Location of translational initiation factor IF3 on the small ribosomal subunit. *Proc Natl Acad Sci U S A* **96**, 4301-4306 (1999).

35. M. M. Yusupov *et al.*, Crystal structure of the ribosome at 5.5 A resolution. *Science* **292**, 883-896 (2001).

36. K. A. Datsenko, B. L. Wanner, One-step inactivation of chromosomal genes in Escherichia coli K-12 using PCR products. *Proc Natl Acad Sci U S A* **97**, 6640-6645 (2000).

37. A. Eudes *et al.*, Production of hydroxycinnamoyl anthranilates from glucose in Escherichia coli. *Microb Cell Fact* **12**, 62 (2013).

38. R. Lutz, H. Bujard, Independent and tight regulation of transcriptional units in Escherichia coli via the LacR/O, the TetR/O and AraC/I1-I2 regulatory elements. *Nucleic Acids Res* **25**, 1203-1210 (1997).

39. D. Yu *et al.*, An efficient recombination system for chromosome engineering in Escherichia coli. *Proc Natl Acad Sci U S A* **97**, 5978-5983 (2000).

40. L. C. Thomason, N. Costantino, D. L. Court, E. coli genome manipulation by P1 transduction. *Curr Protoc Mol Biol* **Chapter 1**, 1 17 11-11 17 18 (2007).

41. Z. T. Laughlin *et al.*, 50S subunit recognition and modification by the Mycobacterium tuberculosis ribosomal RNA methyltransferase TlyA. *Proc Natl Acad Sci U S A* **119**, e2120352119 (2022).

42. K. Miyazaki, MEGAWHOP cloning: a method of creating random mutagenesis libraries via megaprimer PCR of whole plasmids. *Methods Enzymol* **498**, 399-406 (2011).

43. A. Punjani, J. L. Rubinstein, D. J. Fleet, M. A. Brubaker, cryoSPARC: algorithms for rapid unsupervised cryo-EM structure determination. *Nat Methods* **14**, 290-296 (2017).

44. T. D. Goddard *et al.*, UCSF ChimeraX: Meeting modern challenges in visualization and analysis. *Protein Sci* **27**, 14-25 (2018).

45. R. Sanchez-Garcia *et al.*, DeepEMhancer: a deep learning solution for cryo-EM volume post-processing. *Commun Biol* **4**, 874 (2021).

46. E. M. Maksimova *et al.*, RbfA Is Involved in Two Important Stages of 30S Subunit Assembly: Formation of the Central Pseudoknot and Docking of Helix 44 to the Decoding Center. *Int J Mol Sci* **22** (2021).

47. D. Liebschner *et al.*, Macromolecular structure determination using X-rays, neutrons and electrons: recent developments in Phenix. *Acta Crystallogr D Struct Biol* **75**, 861-877 (2019).

48. P. Emsley, K. Cowtan, Coot: model-building tools for molecular graphics. *Acta Crystallogr D Biol Crystallogr* **60**, 2126-2132 (2004).

49. W. L. DeLano, PyMOL: An Open-Source Molecular Graphics Tool. *CCP4 Newsletter on Protein Crystallography*, 82-90 (2002).